

SeasonScapes: Learning Large-scale Re-lightable 3D Landscapes with Seasonal Variation from Sparse Webcams

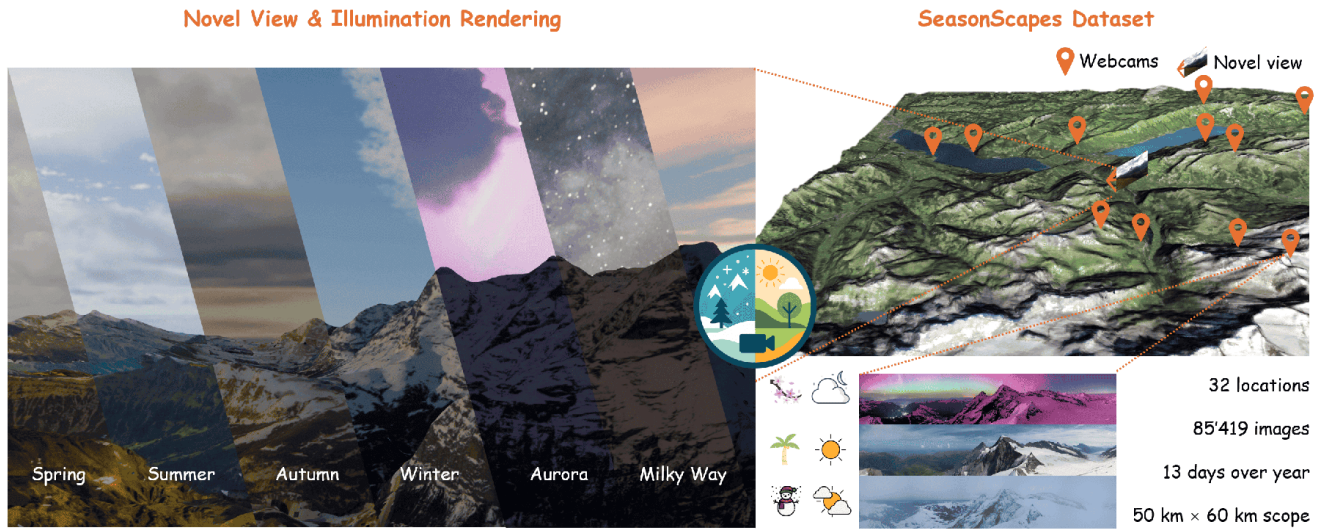
Timo Kleger²Qi Ma^{1,2}Deheng Zhang¹Luc Van Gool¹Danda Pani Paudel¹¹INSAIT, Sofia University “St. Kliment Ohridski”²ETH Zurich

Figure 1. We introduce SeasonScapes framework and a the SeasonScapes dataset: Swiss Sparse-view Mountain Scenes with Seasonal Changes that covers over $50 \text{ km} \times 60 \text{ km}$, composed of more than 85,000 webcam images captured from 32 different locations across 13 timestamps throughout a full year. By projecting these timestamp-specific images onto a 3D mesh, we construct seasonal 3D landscapes that reflect natural appearance changes over time. To address occlusions and missing data, we leverage conditional diffusion models for image-guided inpainting directly on the mesh. The resulting completed meshes can be further relighted using standard physically-based renderer.

Abstract

Large-scale scene creation from sparse views in the wild remains an open and significant problem in computer vision due to challenges such as camera calibration errors, limited scene coverage, and high scene complexity, including lighting and appearance variations. To address this, we introduce a digital twin of the Swiss alpine landscape, capturing temporal variations across seasons and times of day using our newly proposed SeasonScapes dataset for sparse-view mountain scenes with seasonal changes. We associate sparsely distributed webcams across 3000 km^2 of the Bernese Highlands with a low-resolution satellite image and elevation map via 2D–3D correspondence optimization. To overcome limited scene coverage, we propose

a 3D mesh painting method that inpaints novel views using priors from the ControlNet pipeline. Unlike prior works that focus on centered, bounded objects, our approach handles large-scale, unbounded scenes by introducing linear or cubic spline inpainting trajectories between GPS coordinates and performing occlusion-aware painting via UV indexing through depth rendering – rather than relying solely on normal-based filtering. By running the pipeline across varying times of day and seasons, we create a dataset with rich appearance and lighting diversity. Using this data, we train a relightable Gaussian Splat model with appearance Multi-Layer Perceptron.

1. Introduction

Large-scale 3D landscape reconstruction holds substantial importance for real-world applications such as environmental monitoring, weather modeling, virtual tourism, infrastructure planning and disaster response. However, this is a challenging task in computer vision and graphics due to the high variance of the weather, season, and illumination. Beyond traditional mesh-based systems like Google Earth that rely on static geometry and blended satellite texture maps, our work focuses on achieving photometrically consistent 3D representations capable of modeling diverse illumination conditions and view-dependent appearance variations. We leverage known 3D geometry and sparse webcam imagery to reconstruct up-to-date scene states with high visual fidelity.

Existing large-scale 3D datasets primarily target on static urban environments [12, 27, 46], with limited coverage of natural landscapes. These dataset have significantly advanced task like large-scale reconstruction in terms of efficiency, hierarchical scene representation [23, 30, 46] and task like scene understanding and localization [10, 31]. To address this gap, we introduce the SeasonScapes dataset for sparse-view mountain scenes with seasonal and intraday illumination change, covering 3,000 km² of alpine Swiss terrain across 12 months to capture seasonal variations and complete diurnal cycles from dawn to dusk. This spatially and temporally comprehensive dataset enables modeling of both long-term environmental transitions and short-term illumination changes in natural mountain landscapes. We expand upon NeRF-W’s temporal modeling dataset [32] in scope and capability by offering: (1) large-scale natural landscapes rather than isolated urban landmarks; (2) precise timestamp annotations for all webcam observations; (3) calibrated 2D-3D correspondences between ground-level imagery and georeferenced satellite data.

Although prior works [25, 32, 40] tackle 3D reconstruction in unconstrained environments, they do not target large-scale landscape reconstruction from sparsely distributed camera views. We introduce SeasonScapes, a novel framework for reconstructing large-scale, relightable 3D landscapes that capture both seasonal and diurnal variations. Building upon our multimodal dataset, SeasonScapes integrates: macro-scale environmental structures (terrain topography, hydrographic boundaries, and urban infrastructure) with micro-scale dynamic observations (temporal illumination changes, biological activity patterns, and sub-surface features). This approach advances beyond satellite-only reconstruction methods [9, 53], enabling comprehensive spatiotemporal scene understanding across multiple scales.

Our framework generates temporally consistent 3D landscapes with photorealistic lighting—spanning day/night cycles and seasonal variations from summer to winter—using

arbitrary unconstrained webcam inputs. The pipeline begins by texturing the base mesh through projective blending of available 2D observations, then completes missing regions with depth-conditioned diffusion models that leverage optimized inpainting trajectories to preserve spatial consistency. Finally, we train a relightable Gaussian model that employs a multi-layer perceptron to capture dynamic scene properties. Through comprehensive experiments across three diverse test scenes, we demonstrate our method’s ability to render realistic environments while accurately modeling scene dynamics across varying lighting and seasonal conditions.

Our contributions can be summarized as:

- We present SeasonScapes dataset, a high-quality large-scale multimodal dynamic dataset with seasonal and diurnal variations, covering 3,000 km² of alpine terrain.
- We propose SeasonScapes framework for relightable 3D landscape creation that leverages diffusion priors to inpaint unseen regions with high fidelity.
- We incorporate dynamic embeddings into relightable gaussian training, enabling effective modeling of temporal changes in large-scale outdoor scenes.

The source code, configurations, rendered examples and where to download the SeasonScapes dataset are available at: <https://github.com/ChlaegerIO/SeasonScapes>.

2. Related Work

Large-scale Landscape dataset. Early work [6, 12, 37, 42] introduced paired 2D-3D semantic data for scene understanding, but primarily focused on urban and vehicular environments. The RUGD dataset [50] centers on off-road semantic segmentation, subsequent works [16, 47] extend this to 3D scene understanding. However, these datasets remain limited in scale, covering less than 20 km of trajectory data. [4] also introduced dataset featuring alpine region elevation models, demonstrating robust cross-domain camera pose estimation through learned descriptor matching. [47] benchmark the 2D and 3D semantic segmentation. Most closely related to our work is [4] which introduced a dataset featuring alpine region elevation models and demonstrated robust cross-domain camera pose estimation through learned descriptor matching.

Sparse-view mesh colorization. Traditional methods for synthesizing textures on 3D assets typically relied on placing hand-crafted patterns or performing global optimization [15, 24, 45]. More recently, learning-based approaches have demonstrated strong performance in generating plausible textures for complex 3D shapes [8, 20, 39, 44]. One notable method, TEXTure [41], iteratively applies a pre-trained depth-to-image diffusion model to paint the texture map from multiple viewpoints, conditioning each step on previous results. While effective, this approach lacks global context and often produces view-inconsistent textures. Tex-

Fusion [5] addresses this limitation by aggregating texture information across multiple views during the denoising process, thereby improving view consistency. Text2Tex [7] further automates viewpoint selection, reducing manual intervention. Despite these advancements, existing methods still suffer from lighting bias introduced by 2D priors, leading to inconsistent textures under varying illumination. To mitigate this, Paint3D [57] introduces a refinement model trained on illumination-free texture data, significantly reducing lighting artifacts and improving overall consistency. We adapt these diffusion-based texture inpainting techniques to the challenging setting of large-scale landscape reconstruction, achieving photorealistic and view-consistent rendering across varying illumination and viewpoints.

3D Scene editing and relighting. Recent advancements in novel view synthesis [2, 22, 34, 56] have primarily concentrated on static environment reconstruction. Subsequent works [19, 26, 48, 55, 58, 63] have extended this toward 3D scene editing and controllability. Some approaches enable object-level relighting by leveraging 3D distillation of diffusion model [18, 62] or inverse rendering [3, 17, 29, 36, 59], while others address scene-level illumination editing [28, 51, 64]. However, current scene-level relighting methods often struggle to reconstruct the scene under diverse lighting conditions. WildGS [25] addresses this by incorporating DINO v2 features [38] and per-image appearance embeddings [32], enabling faster optimization and robust handling of dynamic scenarios, including illumination changes. These per-image features can further be leveraged to edit lighting conditions at render time. Despite these advances, methods based on 3D Gaussian Splatting (3DGS) [22] often suffer from view overfitting and degrade in quality under sparse camera views, such as those captured from webcams. To address this, our proposed pipeline introduces camera view augmentation.

3. Method

3.1. Preliminary

Diffusion Models. Diffusion models [14, 43] learn complex data distributions by reversing a multi-step noising process. The noising process transforms data samples x into noise over a sequence of $T \in \mathbb{N}$ steps. The model is trained to learn the denoising process.

A Denoising Diffusion Probabilistic Model (DDPM) applies Gaussian noising through T steps with variance schedule β_1, \dots, β_T where:

$$q(x_t | x_{t-1}) = \mathcal{N}(x_t; \sqrt{1 - \beta_t}x_{t-1}, \beta_t\mathbb{I}), \quad (1)$$

where \mathbb{I} is the identity matrix. This schedule ensures x_T approaches an isotropic Gaussian, *i.e.*, $q(x_T) \approx \mathcal{N}(\mathbf{0}, \mathbb{I})$. Setting $\alpha_t = 1 - \beta_t$ and $\bar{\alpha}_t = \prod_{i=1}^t \alpha_i$ yields a closed-

form solution for directly sampling x_t given a data point x_0 :

$$x_t \sim q(x_t | x_0) = \mathcal{N}(x_t; \sqrt{\bar{\alpha}_t}x_0, (1 - \bar{\alpha}_t)\mathbb{I}). \quad (2)$$

For sufficiently small β_t , the reverse $p_\theta(x_{t-1} | x_t)$ is Gaussian. Thus, we approximate it with model \mathcal{F}_{θ_d} :

$$p_\theta(x_{t-1} | x_t) = \mathcal{N}(x_{t-1}; \sqrt{\alpha_t}\mathcal{F}_{\theta_d}(x_t, t), (1 - \alpha_t)\mathbb{I}). \quad (3)$$

ControlNet. Recent advancements to steer diffusion models based on conditional inputs have yielded to astonishing results [11, 33, 35, 52, 60]. One of which is the ControlNet which adds an additional fine-tunable encoder block \mathcal{F}_{θ_c} and zero convolution \mathcal{Z} to the diffusion model \mathcal{F}_{θ_d}

$$\mathcal{F}_\theta = \mathcal{F}_{\theta_d}(x_t, t) + \mathcal{Z}(\mathcal{F}_{\theta_c}(x_t + \mathcal{Z}(c))). \quad (4)$$

The additional encoder block is added to the standard diffusion model with a zero convolution to start fine-tuning from the diffusion model. The additional condition c such as depth, normals, human pose or other control images helps to guide the diffusion model to the desired output.

3D Gaussian Splatting. 3DGS represents scene space with Gaussian primitives $\{Y_i\}_{i=1}^N$, stacking these as follows:

$$Y = [C, O, S, R, SH] \in \mathbb{R}^{N \times 59}, \quad (5)$$

where $C \in \mathbb{R}^{N \times 3}$ denotes the centroid, $O \in \mathbb{R}^{N \times 1}$ the opacity, $S \in \mathbb{R}^{N \times 3}$ the scale, $R \in \mathbb{R}^{N \times 4}$ the quaternion rotation vector, and $SH \in \mathbb{R}^{N \times 48}$ the degree-3 spherical harmonics. Each Gaussian defines a spatial area with opacity. Scene point q is influenced by Gaussian Y_i via opacity-weighted distribution where:

$$h_i(q) = O_i \exp\left(-\frac{1}{2}(q - C_i)^T \Sigma_i^{-1}(q - C_i)\right), \quad (6)$$

where covariance Σ_i is formulated as $\Sigma_i = R_i S_i S_i^T R_i^T$.

Projected onto a 2D image plane, each Gaussian’s influence, h , contributes to a pixel’s color through an alpha-blending equation over the set \mathcal{G} of influencing Gaussians:

$$c_{\text{pixel}} = \sum_{i \in \mathcal{G}} c_i h_i^{2D} \prod_{j=1}^{i-1} (1 - h_j^{2D}). \quad (7)$$

Differentiable rasterization enables gradient-based optimization of Gaussian parameters. In this manner, we represent images rendered from pose P given by $I = \mathcal{G}(P)$.

3.2. Data Preprocessing

We begin by preprocessing the panoramic webcam images and the 3D elevation model as follows:

Initialize 3D Landscape. We start from a low-resolution Digital Elevation Model I_{DEM} and an aerial satellite color

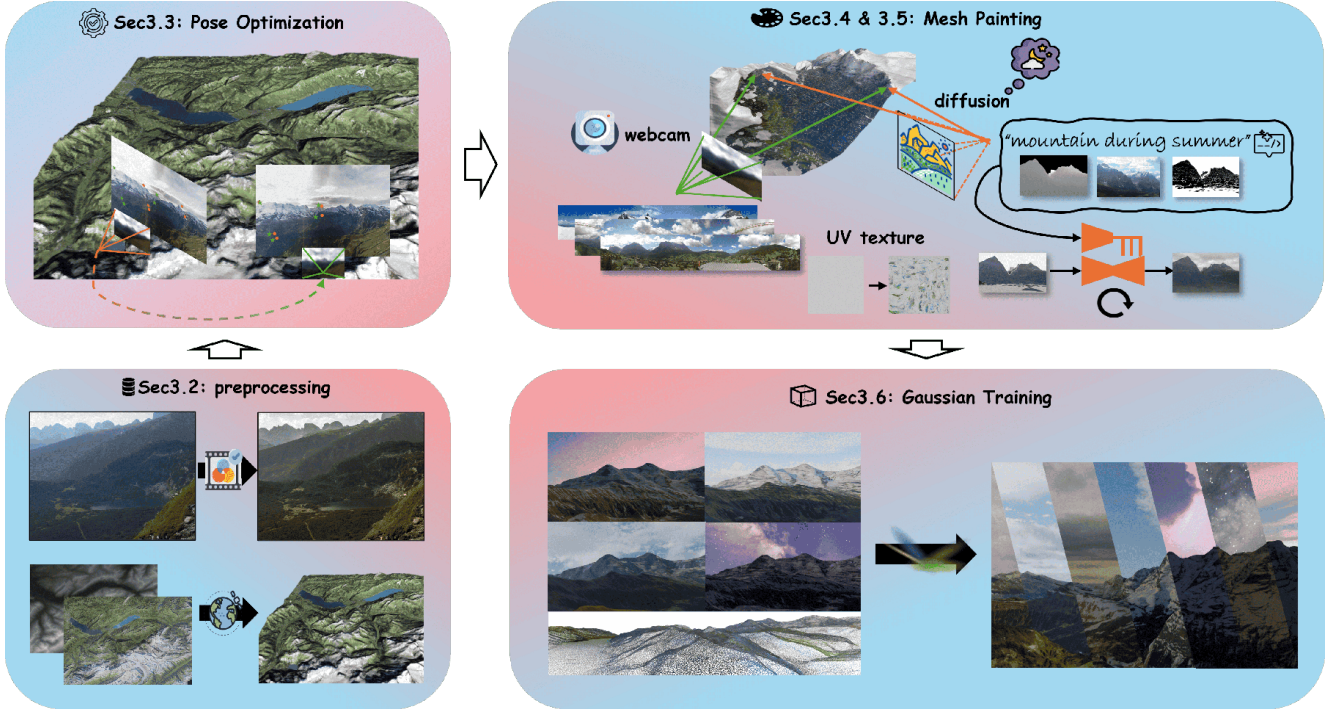


Figure 2. **Pipeline overview.** Our pipeline generates time-varying 3D landscapes through a multi-stage process. First, we preprocess Google Earth data and webcam imagery (Sec. 3.2). We then employ a learning-based approach to optimize camera parameters, aligning the 2D webcam frames with the 3D landscape point cloud (Sec. 3.3). In the landscape painting stage, we project the preprocessed images to texture the UV map (Sec. 3.4). To ensure completeness, we perform mesh inpainting (Sec. 3.5), using an off-the-shelf ControlNet to iteratively fill occluded or missing regions. Finally, after post-processing the UV maps, the outputs from multiple runs are used to supervise the seasonal and diurnal embeddings of a WildGaussian model.

image I_S of our specified region that we downloaded using Google Earth Engine [1]. Then we create a 3D point for each pixel using the normalized height from I_{DEM} and color it with the satellite image I_S . Based on the point cloud we create a mesh using the Poisson surface reconstruction algorithm [21] $M = (V, F)$ with vertices $V = \{v_i\}, v_i \in \mathbb{R}^3$ and triangular faces $F = \{f_i\}, f_i \in \{v_i\}^3$ in the operation $\mathcal{M} : (I_{DEM}, I_S) \mapsto M$.

We unwrap the surface of our 3D mesh using the library xatlas [54] and get the UV texture image $T \in \mathbb{R}^{H \times W \times 3}$ with a predefined resolution. Using a UV map allows texture and appearance information to be stored separately from geometry, enabling efficient reuse across large and complex scenes.

Webcam Preprocessing. Most selected panorama webcams employ a 360° horizontal field of view with cylindrical projection. To align with ControlNet’s planar image processing, we split each webcam feed into 4–6 perspective sub-images facing distinct directions, followed by projection to planar coordinates. For better visualization we additionally color graded the images in Lightroom by adding more contrast, reducing the highlights, elevated shadow levels, and modified white balance toward warmer tones.

3.3. Camera Parameter Optimization

As shown in Fig. 3, given the preprocessed 3D mesh, we associate 3D points with 2D webcam images. While initial poses are estimated from RoundShot camera GPS coordinates, calibration errors persist due to perspective differences (parallax in terrain), limited GPS accuracy ($\pm 3\text{--}10\text{m}$), elevation datum mismatches and temporal drift between satellite/webcam captures. To address this, we first manually establish 3D-to-2D correspondences using custom tools developed with Tkinter. For each matched pair (p_{3D}, p_{2D}) , we optimize learnable camera parameters by minimizing the \mathcal{L}_1 loss between projected 3D points p_{3D} and target 2D points:

$$\mathcal{L}_{\text{pixel}} = \|p_{3D} - p_{2D}\|_1. \quad (8)$$

Since the webcam images are already undistorted, we model the projection using a pinhole camera projection as follows:

$$p_{3D} = \Pi(P_{3D}) = \begin{bmatrix} u \\ v \\ 1 \end{bmatrix} = \begin{bmatrix} f_x & 0 & c_x \\ 0 & f_y & c_y \\ 0 & 0 & 1 \end{bmatrix} \begin{bmatrix} R & t \\ 0 & 1 \end{bmatrix} P_{3D} \quad (9)$$

with focal lengths f_x and f_y , principle point (c_x, c_y) , rotation $R \in \mathbb{R}^{3 \times 3}$ and translation $t \in \mathbb{R}^3$. We optimize the intrinsic camera parameter f_x and f_y and the extrinsic camera parameter for the horizontal rotation.

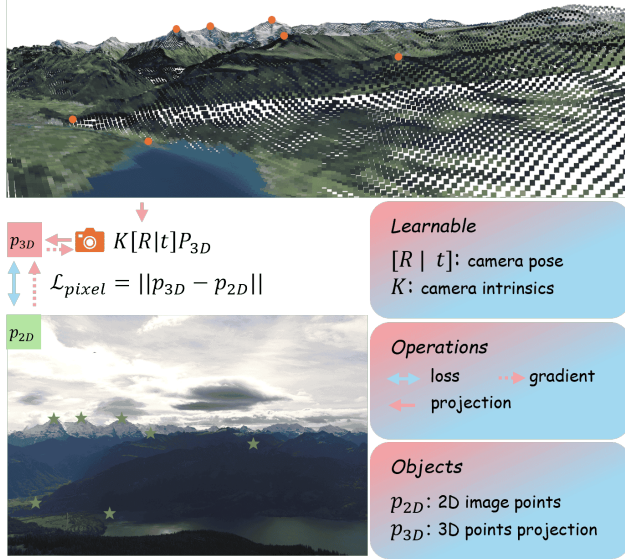


Figure 3. **Camera parameter optimization.** We refine the initial camera intrinsics and extrinsics (derived from GPS coordinates) by calculating the \mathcal{L}_1 pixel loss between the 3D points projection (orange circle) with manually labeled correspondent 2D image points (green).

3.4. Webcam Texturing in UV Space

Our proposed 3D SeasonScapes starts with painting the mesh with our preprocessed webcams I_w (section 3.2) at the optimized pose p_w (section 3.3) and the initialized 3D mesh M_0 with the corresponding texture map T_0 .

Initial Viewpoint. We texture the UV map T_1 (Alg. 1 line 4, 1.4) with the first webcam image I_1 using the pose p_1 and the seen face indices $f_1^{(idx)}$ (Alg. 1.3), denoted as

$$\mathcal{T}_1 : (M_0, I_1, p_1, f_1^{(idx)}, m_0^{UV}) \mapsto T_1. \quad (10)$$

The UV mask m_0^{UV} is one everywhere for the first image.

Painting Viewpoints. The next webcam poses p_t are executed in a similar process \mathcal{T}_t (Alg. 1.4) while taking into account the already textured regions $T_{[1,t-1]}$. Specifically we calculate a UV texture mask m_{t-1}^{UV} of regions in the UV map that are already painted. And then we superpose all previous textures $T_{[1,t-1]}$ with the current texture T_c

$$T_t = m_{t-1}^{UV} \odot T_{t-1} + (1 - m_{t-1}^{UV}) \odot T_c. \quad (11)$$

Therefore the painting is progressively added to the previous texture following Fig. 4 without the inpainting ControlNet and it's inputs until all W webcam views are painted $T_W = T_{[1,W]}$.

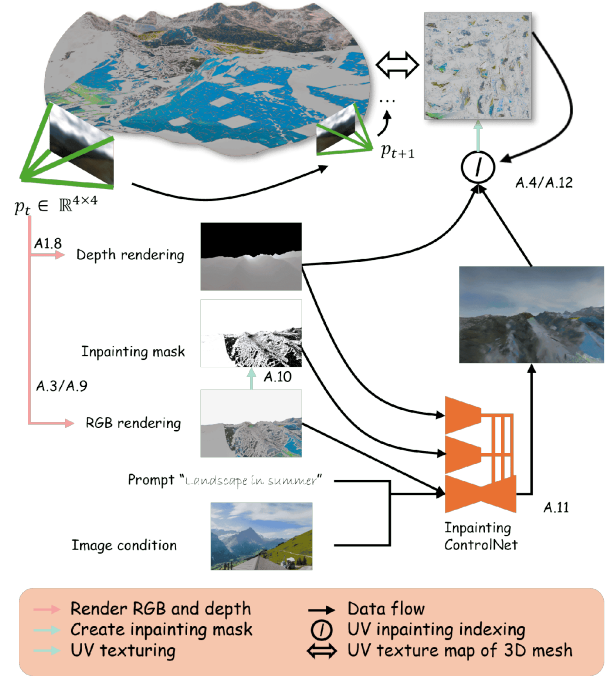


Figure 4. **3D mesh texturing including inpainting.** We iterate over the entire inpainting trajectory $\{p_t\}_{t=1}^N$. For each step t we render an RGBD image. Using the RGB image we mask unseen regions using the HSV color space. We condition ControlNet using the inpainting mask, depth map, text prompt, and IP-Adapter image. The diffusion output is projected onto the UV map via depth-indexing of visible regions. The algorithm description A.1.8 refers to the 8 line of the algorithm 1.

3.5. Iterative Inpainting

In the second step we inpaint missing regions using a depth-aware 2D inpainting diffusion model along a user-specified novel view path with poses $\{p_t\}_{t=1}^N$. We start from the webcam painted texture $T_0 = T_W$ i.e. mesh M_W (Alg. 1.5). As in the painting step we render the depth d_t and visible faces $f_t^{(idx)}$. Additionally we render a partially colored RGB image \tilde{x}_t . The rendering process is described as $\mathcal{R} : (M_{t-1}, p_t) \mapsto (d_t, f_t^{(idx)}, \tilde{x}_t)$ in Alg. 1.8-9. From the RGB image \tilde{x}_t we calculate the uncolored image mask \tilde{x}_m using HSV color space filtering of the background color (Alg. 1.10). These uncolored parts of the image are inpainted with the depth-aware inpainting ControlNet (Alg. 1.11) denoted as

$$x_t = \mathcal{F}_\theta(\tilde{x}_t, \tilde{x}_m, g, d_t; \theta_i, \theta_a, \theta_c), \quad (12)$$

where θ_i is the inpainting ControlNet, θ_a is the IP-Adapter encoder, θ_c is the depth ControlNet and g is the appearance condition of a nearby webcam image and the text prompt. Then the inpainted image is textured onto a local UV texture

map $\mathcal{T}_t : (M_{t-1}, x_t, p_t, f_t^{(idx)}, m_{t-1}^{UV}) \mapsto T_t$ and then superposed with the previous texture map as in equation (11) and Alg. 1.12. After the loop we return the inpainted UV texture $T_I = T_N$ (Alg. 1.13), do a UV texture postprocessing to fill the remaining regions and save the inpainted frames and create a video. Or the inpainted images from several timestamps are used in section 3.6 to train a Wild Gaussian 3D scene.

Algorithm 1 SeasonScapes Training

Require:

Inputs:

- Webcam images I_w and pose p_w
- Uncolored 3D mesh M_0 with UV texture T_0
- Inpainting path with poses $\{p_t\}_{t=1}^N$
- Diffusion parameters $\mathcal{F}_{\theta_d}, \mathcal{F}_{\theta_c}, \mathcal{F}_{\theta_i}, \mathcal{F}_{\theta_a}$
- Text, IP-Image guidance g

Ensure: Estimate the UV texture T

```

1: for  $t = 1$  to  $W$  do
2:   # Paint
3:   Render valid face indices:  $f_t^{(idx)} \leftarrow \mathcal{R}(M, p_t)$ 
4:   Texture:  $T_t \leftarrow \mathcal{T}(M_{t-1}, I_t, f_t^{(idx)}, m_{t-1}^{UV})$ 
5:  $T_0 \leftarrow T_W, M_0 \leftarrow M_W$ 
6: for  $t = 1$  to  $N$  do
7:   # Inpaint
8:   Render depth, face indices:  $d_t, f_t^{(idx)} \leftarrow \mathcal{R}(M, p_t)$ 
9:   Render RGB:  $\tilde{x}_t \leftarrow \mathcal{R}(M_{t-1}, p_t)$ 
10:  Mask RGB:  $\tilde{x}_m \leftarrow \text{Mask}(\tilde{x}_t)$ 
11:  Inpaint:  $x_t \leftarrow \mathcal{F}_\theta(\tilde{x}_t, \tilde{x}_m, g, d_t; \theta_i, \theta_a, \theta_c)$ 
12:  Texture:  $T_t \leftarrow \mathcal{T}(M_{t-1}, x_t, f_t^{(idx)}, m_{t-1}^{UV})$ 
13: return  $T_I$ 

```

3.6. Time Embedding using Wild Gaussian

After performing inpainting on the sparse input views, we obtain denser camera views along the trajectory. By repeating this process across multiple timestamps, we generate images with both spatial and temporal variations. These images, combined with 3D mesh, are then used for training re-lightable Gaussians within the wWild Gaussian framework with learned time embeddings as stated in Kulhanek et al. [25]. The color attributes of each 3D Gaussian, denoted as $\hat{c}_i(r)$, are transformed via an affine operation parameterized by an appearance MLP. $\tilde{c}_i = \gamma \cdot \hat{c}_i(r) + \beta$. The MLP outputs coefficients $(\beta, \gamma) \in (\mathbb{R}^3, \mathbb{R}^3)$ conditioned on the viewing ray direction. r .

4. Experiments

To evaluate our SeasonScapes pipeline, we present both qualitative comparisons against Google Earth’s visual outputs and quantitative metrics of our pipeline. Firstly, we introduce the dataset settings and evaluation metrics. Then

we conduct an ablation study to demonstrate the effectiveness of each module in our framework.

Evaluation Procedure. We evaluate the inpainted images with commonly used metrics for reconstruction quality. Specifically we report the the Learned Perceptual Image Patch Similarity (LPIPS) with AlexNet [61], Peak-Signal-to-Noise Ratio (PSNR) and Structural Similarity Index Measure (SSIM) [49]. We prioritize the LPIPS metric for evaluation because our test views combine visible regions from the initial viewpoint with unseen areas requiring plausible appearance synthesis. Unlike pixel-level metrics that fail to assess generated content meaningfully, LPIPS effectively measures perceptual similarity for real and synthesized regions, ideal for mixed-scenario validation. To calculate the score we render inpainted images in the resolution of 1024×1536 at the webcam location and compare them to the actual webcam. As the sky with the clouds are artificially generated we mask out the sky and the near region as the webcams often has houses here.

4.1. Quantitative and Qualitative Evaluation

We evaluate our 3D landscape texturing in 3 different areas of the 3D mesh. The first Grindelwald scene is a small scene with one mountain that is viewed from different directions. Whereas the Jungfrau scene consists of several mountains and valleys and is painted with 14 webcam images. The last scene consists of a large part of the Bernese highlands with $21 \text{ km} \times 36.5 \text{ km}$. In case of the Grindelwald scene we average 18 different timestamps and we get a LPIPS value of 0.159. In case of the larger Jungfrau scene with 14 different timestamps this value increase to 0.191, as seen in Tab. 1 and for the Bernese highland scene with 4 different timestamps we get a LPIPS of 0.216. The performance degradation is primarily attribute to increased unseen regions in evaluation views. We provide detailed analysis and visual examples demonstrating the quality variation between optimally and poorly rendered regions.

Table 1. **Quantitative evaluation.** We list a small scene, Grindelwald, which consists of 2 painting views and 1 evaluation view per timestamp and a larger scene, Jungfrau region, that has 14 painting views and 41 evaluation views for each timestamp. The number of inpainting view N appears in parentheses after each scene name.

Region	LPIPS ↓	PSNR ↑	SSIM ↑
Grindelwald (54)	0.159	20.56	0.86
Jungfrau (674)	0.191	18.58	0.831
Bern high (168)	0.216	19.20	0.804

We qualitatively compare the ground truth webcam images and our inpainted renderings in Fig. 5. To ensure a rigorous evaluation of topographic reconstruction, we apply a binary mask to the sky and foreground regions, thereby isolating the mountain facets and mitigating the impact of

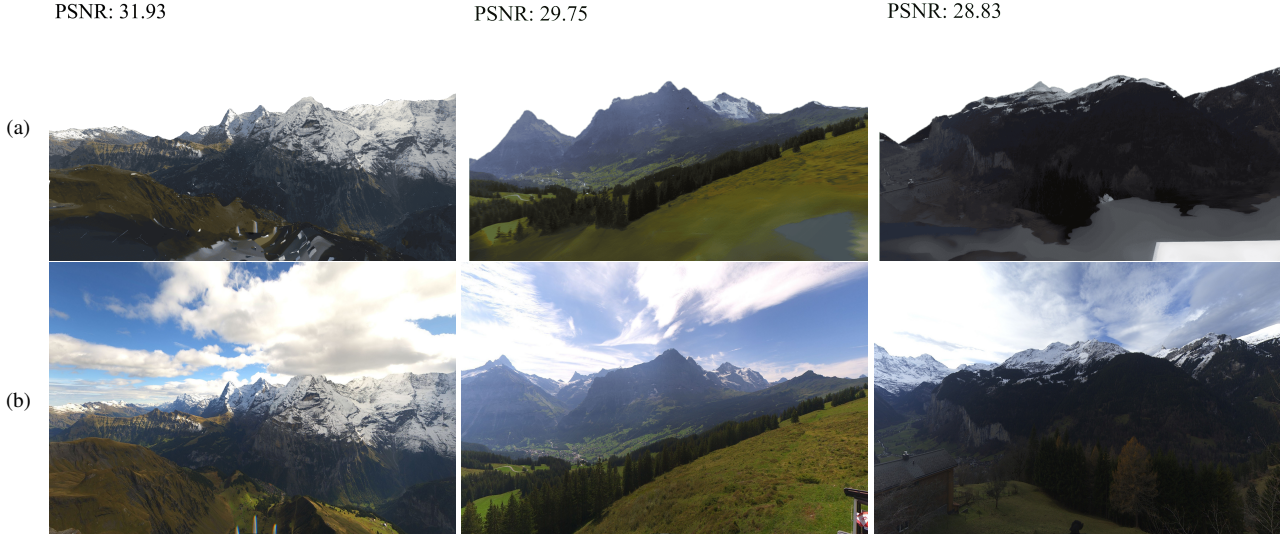


Figure 5. **Qualitative comparison.** (a) shows the inpainted images from our 3D landscape mesh without the clouds and in row (b) are the ground truth webcam images. The evaluation is done without the sky and without the nearest parts of the mesh. The first image is from the 7.10.2024 at 12 AM, the second image is from the 20.7.2024 at 12 AM, third image is from the 7.12.2024 at 12 AM.

painting-related artifacts in the near-field from skewing the quantitative results. on the PSNR calculation. Results demonstrate consistent artifacts in region which is fully painted by ControlNet, like the valley region in first column, the grassy area and the forested zone in second and third column.

4.2. Ablation Studies

We perform an ablation study of our SeasonScapes pipeline, systematically removing components and analyzing their impact through quantitative metrics in Tab. 2 and qualitatively in Fig. 7.

We observe a significant performance drop when skipping the first-stage painting initialization in both scenes. Note that the performance drop is more pronounced in the Grindelwald scene compared to the Jungfrau region. We attribute this to the Jungfrau’s primary bottleneck being its extensive unseen areas and overall lower quality - where synthesized content dominates and control signals have reduced impact. This observation is supported by comparable LPIPS results despite noticeable pixel-level performance drops. In Fig. 7 the result demonstrate that omitting depth control leads to mountain hallucinations in distant regions and the IP-Adapter mainly primarily modulates color tones in the synthesized image.

4.3. Qualitative Comparison with Google Earth

In Fig. 6 we compare our results with rendered 3D Landscape from Google Earth. Our method demonstrates superior coloring of steep cliff faces by better capturing near-orthogonal views, in contrast to Google Earth’s satellite-

Table 2. **Quantitative results of the ablation study.** We evaluate how different control conditions affect performance across both the smaller scale Grindelwald scene and larger scale Jungfrau region, with detailed qualitative explanation shown in Fig. 7.

Ablation study	LPIPS↓	PSNR↑	SSIM↑	Drop
Grindelwald 1. September 2024				
All	0.145	23.02	0.889	
W/o prompt	0.149	22.92	0.886	2.8 %
W/o depth cNet	0.150	22.56	0.884	3.5 %
W/o inpaint mask	0.152	22.43	0.882	4.8 %
W/o IP-Adapter	0.148	22.03	0.880	2.0 %
W/o paint	0.193	19.40	0.863	33.1 %
Jungfrau region 1. September 2024				
All	0.184	19.65	0.833	
W/o prompt	0.183	19.66	0.832	-0.5 %
W/o depth cNet	0.185	19.57	0.830	0.5 %
W/o inpaint mask	0.183	19.38	0.829	-0.5 %
W/o IP-Adapter	0.184	19.65	0.832	0.0 %
W/o paint	0.206	18.02	0.830	12.0 %

based perspective, which often misses details on vertical surfaces due to its top-down viewpoint and warping. Furthermore, our method adapts more efficiently to seasonal variations due to reduced weather dependency. These results suggest that our approach effectively synthesizes high-fidelity textures especially for vertical topographies.

4.4. Wild Gaussian

In Fig. 8 we show the results of novel-view using wild Gaussian. Since our relightable Gaussian model is trained using

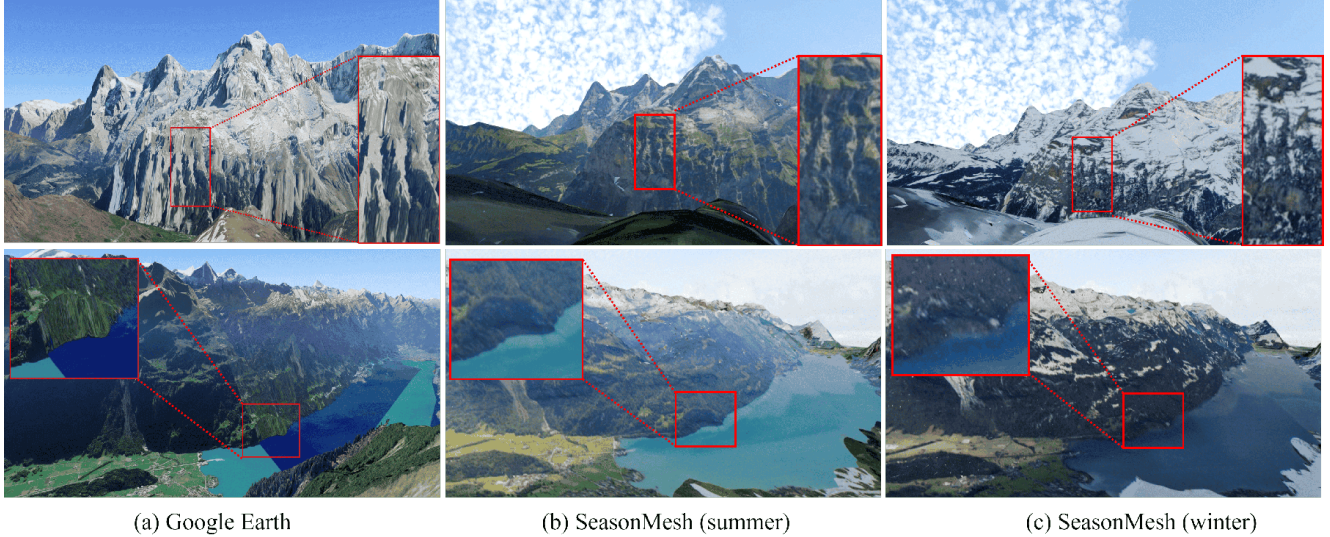


Figure 6. **Qualitative comparison between our approach and Google Earth.** Images (a) are from Google Earth [13], images (b) are our SeasonScapes rendering from the 1.9.2024 at 12 AM, images (c) are our SeasonScapes from the 18.12.2025 at 10 AM. SeasonScapes shows superior photorealistic rendering and time variant ability

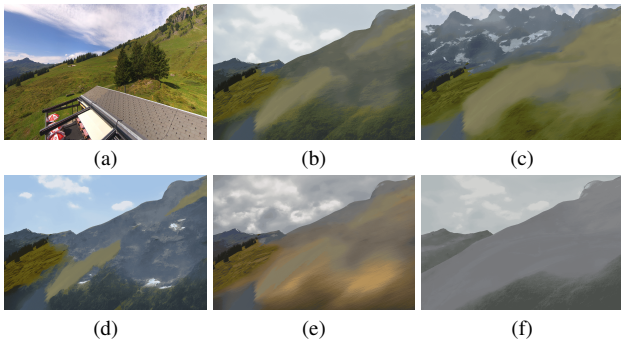


Figure 7. **Qualitative comparison of ablation study.** We evaluate six configurations: (a) target webcam, (b) with all condition, (c) without depth condition, (d) without inpainting mask condition, (e) without IP-Adapter image condition and (f) no initial painting stage.

synthesized ControlNet outputs along a trajectory, we primarily evaluate qualitative performance. The rendered images successfully capture both the structural and appearance variations across different timestamps.

5. Conclusion

We introduce SeasonScapes dataset, a 3D landscape dataset and the corresponding painting pipeline that textures meshes using webcam images while iteratively inpainting missing regions along novel camera trajectories through inpainting ControlNet. The approach robustly adapts to seasonal and diurnal variations by combining multi-source inputs - webcam images, low-resolution digital elevation

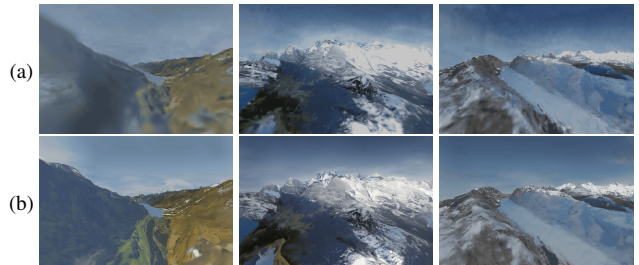


Figure 8. **Qualitative comparison of novel Wild Gaussian views.** (a) Rendered relightable Gaussian outputs and (b) are the inpainted images from our iterative inpainting result. The first and the last image is from the 18.5.2025 at 2 PM, the second image is from the 12.5.2024 at 12 AM.

models (DEMs), and satellite imagery - with camera parameter optimization. We additionally train a relightable Gaussian model using trajectory views, demonstrating robust performance in capturing diverse lighting conditions and appearance variations.

Our approach currently faces several limitations. The manual 2D-3D correspondence process remains time-consuming, and we observe unsatisfactory performance in ControlNet’s ability to inpaint small missing regions. Additionally, the relightable Gaussian outputs occasionally exhibit blurry artifacts, likely due to calibration errors and inherent expressiveness constraints of the Wild Gaussian framework. These limitations present clear directions for future improvement.

Acknowledgments

This research was partially funded by the Ministry of Education and Science of Bulgaria (support for INSAIT, part of the Bulgarian National Roadmap for Research Infrastructure). We would like to thank the company Roundshot for providing the panoramic webcam images.

References

- [1] Guillaume Attard. An Intro to the Earth Engine Python API, 2025. <https://developers.google.com/earth-engine/tutorials/community/intro-to-python-api>. 4
- [2] Jonathan T. Barron, Ben Mildenhall, Dor Verbin, Pratul P. Srinivasan, and Peter Hedman. Mip-nerf 360: Unbounded anti-aliased neural radiance fields, 2022. 3
- [3] Mark Boss, Raphael Braun, Varun Jampani, Jonathan T. Barron, Ce Liu, and Hendrik P.A. Lensch. Nerf: Neural reflectance decomposition from image collections. In *ICCV*, 2021. 3
- [4] Jan Brejcha, Michal Lukáč, Yannick Hold-Geoffroy, Oliver Wang, and Martin Čadík. Landscapear: Large scale outdoor augmented reality by matching photographs with terrain models using learned descriptors. In *European Conference on Computer Vision*, pages 295–312. Springer, 2020. 2
- [5] Tianshi Cao, Karsten Kreis, Sanja Fidler, Nicholas Sharp, and Kangxue Yin. Textfusion: Synthesizing 3d textures with text-guided image diffusion models, 2023. 3
- [6] D. Chen, G. Baatz, Köser, S. Tsai, R. Vedantham, T. Pylvanainen, K. Roimela, X. Chen, J. Bach and M. Pollefeys, B. Girod, and R. Grzeszczuk. City-scale landmark identification on mobile devices. In *Proceedings of Computer Vision and Pattern Recognition (CVPR)*, 2011. 2
- [7] Dave Zhenyu Chen, Yawar Siddiqui, Hsin-Ying Lee, Sergey Tulyakov, and Matthias Nießner. Text2tex: Text-driven texture synthesis via diffusion models, 2023. 3
- [8] Yiwen Chen, Chi Zhang, Xiaofeng Yang, Zhongang Cai, Gang Yu, Lei Yang, and Guosheng Lin. It3d: Improved text-to-3d generation with explicit view synthesis, 2023. 2
- [9] Gabriele Facciolo, Carlo De Franchis, and Enric Meinhardt-Llopis. Automatic 3d reconstruction from multi-date satellite images, 2017. 2
- [10] Jie Feng, Tianhui Liu, Yuwei Du, Siqi Guo, Yuming Lin, and Yong Li. Citygpt: Empowering urban spatial cognition of large language models, 2025. 2
- [11] Rinon Gal, Yuval Alaluf, Yuval Atzmon, Or Patashnik, Amit H. Bermano, Gal Chechik, and Daniel Cohen-Or. An image is worth one word: Personalizing text-to-image generation using textual inversion, 2022. 3
- [12] Andreas Geiger, Philip Lenz, Christoph Stiller, and Raquel Urtasun. Vision meets robotics: The kitti dataset. *International Journal of Robotics Research (IJRR)*, 2013. 2
- [13] Google. Google Earth, 2025. <https://earth.google.com>. 8
- [14] Jonathan Ho, Ajay Jain, and Pieter Abbeel. Denoising diffusion probabilistic models. In *NeurIPS*, pages 6840–6851, 2020. 3
- [15] Jingwei Huang, Justus Thies, Angela Dai, Abhijit Kundu, Chiyu Max Jiang, Leonidas Guibas, Matthias Nießner, and Thomas Funkhouser. Adversarial texture optimization from rgb-d scans, 2020. 2
- [16] Peng Jiang, Philip Osteen, Maggie Wigness, and Srikanth Saripalli. Rellis-3d dataset: Data, benchmarks and analysis, 2020. 2
- [17] Haian Jin, Isabella Liu, Peijia Xu, Xiaoshuai Zhang, Songfang Han, Sai Bi, Xiaowei Zhou, Zexiang Xu, and Hao Su. Tensor: Tensorial inverse rendering. In *CVPR*, 2023. 3
- [18] Haian Jin, Yuan Li, Fujun Luan, Yuanbo Xiangli, Sai Bi, Kai Zhang, Zexiang Xu, Jin Sun, and Noah Snaveley. Neural gaffer: Relighting any object via diffusion. In *Advances in Neural Information Processing Systems*, 2024. 3
- [19] Kacper Kania, Kwang Moo Yi, Marek Kowalski, Tomasz Trzcíński, and Andrea Tagliasacchi. Conerf: Controllable neural radiance fields. In *Proceedings of the IEEE/CVF Conference on Computer Vision and Pattern Recognition*, pages 18623–18632, 2022. 3
- [20] Animesh Karnear, Niloy J. Mitra, Andrea Vedaldi, and David Novotny. Holofusion: Towards photo-realistic 3d generative modeling, 2023. 2
- [21] Michael Kazhdan and Hugues Hoppe. Screened Poisson Surface Reconstruction. *ACM Transactions on Graphics*, 32, 2013. 4
- [22] Bernhard Kerbl, Georgios Kopanas, Thomas Leimkühler, and George Drettakis. 3d gaussian splatting for real-time radiance field rendering, 2023. 3
- [23] Bernhard Kerbl, Andreas Meuleman, Georgios Kopanas, Michael Wimmer, Alexandre Lanvin, and George Drettakis. A hierarchical 3d gaussian representation for real-time rendering of very large datasets. *ACM Transactions on Graphics*, 43(4), 2024. 2
- [24] Johannes Kopf, Chi-Wing Fu, Daniel Cohen-Or, Oliver Deussen, Dani Lischinski, and Tien-Tsin Wong. Solid texture synthesis from 2d exemplars. *ACM Transactions on Graphics (Proceedings of SIGGRAPH 2007)*, 26(3):2:1–2:9, 2007. 2
- [25] Jonas Kulhanek, Songyou Peng, Zuzana Kukelova, Marc Pollefeys, and Torsten Sattler. Wildgaussians: 3d gaussian splatting in the wild, 2024. 2, 3, 6
- [26] Verica Lazova, Vladimir Guzov, Kyle Olszewski, Sergey Tulyakov, and Gerard Pons-Moll. Control-nerf: Editable feature volumes for scene rendering and manipulation. In *Proceedings of the IEEE/CVF Winter Conference on Applications of Computer Vision*, pages 4340–4350, 2023. 3
- [27] Yixuan Li, Lihan Jiang, Linning Xu, Yuanbo Xiangli, Zhenzhi Wang, Dahua Lin, and Bo Dai. Matrixcity: A large-scale city dataset for city-scale neural rendering and beyond. In *Proceedings of the IEEE/CVF International Conference on Computer Vision*, pages 3205–3215, 2023. 2
- [28] Zhihao Liang, Hongdong Li, Kui Jia, Kailing Guo, and Qi Zhang. Gus-ir: Gaussian splatting with unified shading for inverse rendering, 2024. 3
- [29] Zhihao Liang, Qi Zhang, Ying Feng, Ying Shan, and Kui Jia. Gs-ir: 3d gaussian splatting for inverse rendering. In *CVPR*, 2024. 3

- [30] Yang Liu, Chuanchen Luo, Lue Fan, Naiyan Wang, Junran Peng, and Zhaoxiang Zhang. Citygaussian: Real-time high-quality large-scale scene rendering with gaussians. In *European Conference on Computer Vision*, pages 265–282. Springer, 2025. 2
- [31] Qi Ma, Runyi Yang, Bin Ren, Nicu Sebe, Ender Konukoglu, Luc Van Gool, and Danda Pani Paudel. Cityloc: 6dof pose distributional localization for text descriptions in large-scale scenes with gaussian representation, 2025. 2
- [32] Ricardo Martin-Brualla, Noha Radwan, Mehdi S. M. Sajjadi, Jonathan T. Barron, Alexey Dosovitskiy, and Daniel Duckworth. NeRF in the Wild: Neural Radiance Fields for Unconstrained Photo Collections. In *CVPR*, 2021. 2, 3
- [33] Chenlin Meng, Yutong He, Yang Song, Jiaming Song, Jiajun Wu, Jun-Yan Zhu, and Stefano Ermon. Sedit: Guided image synthesis and editing with stochastic differential equations, 2022. 3
- [34] Ben Mildenhall, Pratul P. Srinivasan, Matthew Tancik, Jonathan T. Barron, Ravi Ramamoorthi, and Ren Ng. Nerf: Representing scenes as neural radiance fields for view synthesis, 2020. 3
- [35] Chong Mou, Xintao Wang, Liangbin Xie, Yanze Wu, Jian Zhang, Zhongang Qi, Ying Shan, and Xiaohu Qie. T2i-adapter: Learning adapters to dig out more controllable ability for text-to-image diffusion models, 2023. 3
- [36] Jacob Munkberg, Jon Hasselgren, Tianchang Shen, Jun Gao, Wenzheng Chen, Alex Evans, Thomas Müller, and Sanja Fidler. Extracting triangular 3d models, materials, and lighting from images. In *CVPR*, 2022. 3
- [37] Sarah Taghavi Namin, Mohammad Najafi, Mathieu Salzmann, and Lars Petersson. A multi-modal graphical model for scene analysis. In *2015 IEEE Winter Conference on Applications of Computer Vision*, pages 1006–1013. IEEE, 2015. 2
- [38] Maxime Oquab, Timothée Darcet, Théo Moutakanni, Huy Vo, Marc Szafraniec, Vasil Khalidov, Pierre Fernandez, Daniel Haziza, Francisco Massa, Alaaeldin El-Nouby, Mahmoud Assran, Nicolas Ballas, Wojciech Galuba, Russell Howes, Po-Yao Huang, Shang-Wen Li, Ishan Misra, Michael Rabbat, Vasu Sharma, Gabriel Synnaeve, Hu Xu, Hervé Jegou, Julien Mairal, Patrick Labatut, Armand Joulin, and Piotr Bojanowski. Dinov2: Learning robust visual features without supervision, 2024. 3
- [39] Guocheng Qian, Jinjie Mai, Abdullah Hamdi, Jian Ren, Aliaksandr Siarohin, Bing Li, Hsin-Ying Lee, Ivan Skokhodov, Peter Wonka, Sergey Tulyakov, and Bernard Ghanem. Magic123: One image to high-quality 3d object generation using both 2d and 3d diffusion priors, 2023. 2
- [40] Weining Ren, Zihan Zhu, Boyang Sun, Jiaqi Chen, Marc Pollefeys, and Songyou Peng. Nerf on-the-go: Exploiting uncertainty for distractor-free nerfs in the wild, 2024. 2
- [41] Elad Richardson, Gal Metzer, Yuval Alaluf, Raja Giryes, and Daniel Cohen-Or. Texture: Text-guided texturing of 3d shapes, 2023. 2
- [42] Olivier Saurer, Georges Baatz, Kevin Köser, L’ubor Ladický, and Marc Pollefeys. Image based geo-localization in the alps, 2015. 2
- [43] Jascha Sohl-Dickstein, Eric Weiss, Niru Maheswaranathan, and Surya Ganguli. Deep unsupervised learning using nonequilibrium thermodynamics. In *ICML*, pages 2256–2265, 2015. 3
- [44] Junshu Tang, Tengfei Wang, Bo Zhang, Ting Zhang, Ran Yi, Lizhuang Ma, and Dong Chen. Make-it-3d: High-fidelity 3d creation from a single image with diffusion prior, 2023. 2
- [45] Greg Turk. Texture synthesis on surfaces. In *Proceedings of the 28th Annual Conference on Computer Graphics and Interactive Techniques*, page 347–354, New York, NY, USA, 2001. Association for Computing Machinery. 2
- [46] Haithem Turki, Deva Ramanan, and Mahadev Satyanarayanan. Mega-nerf: Scalable construction of large-scale nerfs for virtual fly-throughs. In *Proceedings of the IEEE/CVF Conference on Computer Vision and Pattern Recognition (CVPR)*, pages 12922–12931, 2022. 2
- [47] Kavisha Vidanapathirana, Joshua Knights, Stephen Hausler, Mark Cox, Milad Ramezani, Jason Jooste, Ethan Griffiths, Shaheer Mohamed, Sridha Sridharan, Clinton Fookes, and Peyman Moghadam. Wildscenes: A benchmark for 2d and 3d semantic segmentation in large-scale natural environments. *The International Journal of Robotics Research*, 44(4):532–549, 2025. 2
- [48] Can Wang, Menglei Chai, Mingming He, Dongdong Chen, and Jing Liao. Clip-nerf: Text-and-image driven manipulation of neural radiance fields. In *Proceedings of the IEEE/CVF Conference on Computer Vision and Pattern Recognition*, pages 3835–3844, 2022. 3
- [49] Zhou Wang, Eero P Simoncelli, and Alan C Bovik. Multi-scale structural similarity for image quality assessment. *The Thirty-Seventh Asilomar Conference on Signals, Systems & Computers*, 2:1398–1402, 2003. 6
- [50] Maggie Wigness, Sungmin Eum, John G Rogers, David Han, and Heesung Kwon. A rugd dataset for autonomous navigation and visual perception in unstructured outdoor environments. In *International Conference on Intelligent Robots and Systems (IROS)*, 2019. 2
- [51] Zirui Wu, Jianteng Chen, Laijian Li, Shaoteng Wu, Zhikai Zhu, Kang Xu, Martin R. Oswald, and Jie Song. 3d gaussian inverse rendering with approximated global illumination, 2025. 3
- [52] Hu Ye, Jun Zhang, Sibio Liu, Xiao Han, and Wei Yang. Ip-adapter: Text compatible image prompt adapter for text-to-image diffusion models, 2023. 3
- [53] Tim Yngesjö. 3d reconstruction from satellite imagery using deep learning. Master’s thesis, Linköping University, Department of Electrical Engineering, Computer Vision, 2021. 2
- [54] Jonathan Young. xatlas: Mesh parameterization / uv unwrapping library, 2022. 4
- [55] Haitao Yu, Deheng Zhang, Peiyuan Xie, and Tianyi Zhang. Point-based radiance fields for controllable human motion synthesis, 2023. 3
- [56] Zehao Yu, Anpei Chen, Binbin Huang, Torsten Sattler, and Andreas Geiger. Mip-splatting: Alias-free 3d gaussian splatting, 2023. 3
- [57] Xianfang Zeng, Xin Chen, Zhongqi Qi, Wen Liu, Zibo Zhao, Zhibin Wang, Bin Fu, Yong Liu, and Gang Yu. Paint3d:

- Paint anything 3d with lighting-less texture diffusion models, 2023. [3](#)
- [58] Deheng Zhang, Clara Fernandez-Labrador, and Christopher Schroers. Coarf: Controllable 3d artistic style transfer for radiance fields, 2024. [3](#)
- [59] Deheng Zhang, Jingyu Wang, Shaofei Wang, Marko Mihajlovic, Sergey Prokudin, Hendrik Lensch, and Siyu Tang. Rise-sdf: A relightable information-shared signed distance field for glossy object inverse rendering. In *International Conference on 3D Vision (3DV)*, 2025. [3](#)
- [60] Lvmin Zhang, Anyi Rao, and Maneesh Agrawala. Adding conditional control to text-to-image diffusion models. In *2023 IEEE/CVF International Conference on Computer Vision (ICCV)*, pages 3813–3824, 2023. [3](#)
- [61] Richard Zhang, Phillip Isola, Alexei A Efros, Eli Shechtman, and Oliver Wang. The unreasonable effectiveness of deep features as a perceptual metric. *CVPR*, 2018. [6](#)
- [62] Xiaoming Zhao, Pratul P. Srinivasan, Dor Verbin, Keunhong Park, Ricardo Martin Brualla, and Philipp Henzler. IllumiNeRF: 3D Relighting Without Inverse Rendering. In *NeurIPS*, 2024. [3](#)
- [63] Yuhang Zheng, Xiangyu Chen, Yupeng Zheng, Songen Gu, Runyi Yang, Bu Jin, Pengfei Li, Chengliang Zhong, Zengmao Wang, Lina Liu, et al. Gaussiangrasper: 3d language gaussian splatting for open-vocabulary robotic grasping. *arXiv preprint arXiv:2403.09637*, 2024. [3](#)
- [64] Jingsen Zhu, Yuchi Huo, Qi Ye, Fujun Luan, Jifan Li, Dianbing Xi, Lisha Wang, Rui Tang, Wei Hua, Hujun Bao, et al. I2-sdf: Intrinsic indoor scene reconstruction and editing via raytracing in neural sdf. In *Proceedings of the IEEE/CVF Conference on Computer Vision and Pattern Recognition*, pages 12489–12498, 2023. [3](#)